Hindawi
Complexity
Volume 2020, Article ID 4627597, 13 pages
https://doi.org/10.1155/2020/4627597

Research Article

Modeling, Synchronization, and FPGA Implementation of Hamiltonian Conservative Hyperchaos

Enzeng Dong,[1] **Xiaodong Jiao**,[1] **Shengzhi Du**,[2] **Zengqiang Chen**,[3] **and Guoyuan Qi**[4]

[1]*Key Laboratory for Control Theory & Applications in Complicated Systems, Tianjin University of Technology, Tianjin 300384, China*
[2]*Department of Mechanical Engineering, Tshwane University of Technology, Pretoria 0001, South Africa*
[3]*Department of Automation, Nankai University, Tianjin 300071, China*
[4]*Tianjin Key Laboratory of Advanced Technology of Electrical Engineering and Energy, Tiangong University, Tianjin 300387, China*

Correspondence should be addressed to Enzeng Dong; dongenzeng@163.com

Received 18 January 2020; Revised 20 March 2020; Accepted 27 March 2020; Published 25 April 2020

Guest Editor: Chun-Lai Li

Conservative chaotic systems have potentials in engineering application because of their superiority over the dissipative systems in terms of ergodicity and integer dimension. In this paper, five-dimension Euler equations are constructed by integrating two of sub-Euler equations, which are contributory to the exploration of higher-dimensional systems. These Euler equations compose the conservative parts from their antisymmetric structure, which have been proved to be both Hamiltonian and Casimir energy conservative. Furthermore, a family of Hamiltonian conservative hyperchaotic systems are proposed by breaking the conservation of Casimir energy. The numerical analysis shows that the system displays some interesting behaviors, such as the coexistence of quasi-periodic, chaotic, and hyperchaotic behaviors. Adaptive synchronization method is used to realize the hyperchaos synchronization. Finally, the system passed the NIST tests successfully. Field programmable gate array (FPGA) platform is used to implement the proposed Hamiltonian conservative hyperchaos.

1. Introduction

Since the discovery of Lorenz attractor in 1963 [1], the interesting dynamic behavior of chaotic attractors has attracted intensive attention, with various mathematical analyses. Conventional analyses on the chaotic system include the determination of Lyapunov exponents (LEs), bifurcation diagram [2], phase portrait, ultimate boundary estimation, and topological horseshoe analysis [3, 4], which illustrate the chaotic state intuitively. LEs are commonly used as an indicator of chaotic systems. The bifurcation diagram focuses on the evolution of the dynamics of a chaotic system when parameters or initial values are changed. The phase portrait describes the phase space trajectory of a chaotic system. The ultimate boundary estimation and topological horseshoe analysis [3, 4] reveal the abundant characteristics of a chaotic system.

Generally, chaotic systems can be categorized into dissipative or conservative chaotic systems. A dissipative chaotic system (DCS) owns strange attractor that has sensitive dependence on initial conditions. A conservative chaotic system (CCS) does not even have any attractor with integer dimension. The ergodicity of CCS is usually greater than DCS. According to the sign of the coefficients in the dissipation term, the DCS can be further divided into two types: Rayleigh and non-Rayleigh DCSs [5, 6], as there must be at least one positive dissipation term in a non-Rayleigh DCS [5]. There are two types of CCSs too. A Hamiltonian CCS (HCCS) meets conditions of zero-sum LEs, and the Hamiltonian energy and the phase space volume are both conservative, while a non-Hamiltonian CCS (non-HCCS) only meets zero-sum LE condition, such as Sprott A system in [7] and Cang-case B system in [8]. HCCSs are further categorized to traditional HCCS (traditional-HCCS) [9, 10]

and generalized HCCS (generalized-HCCS) [11]. DCS has received intensive attention but much little for CCS. In the early stage of chaos research, there are few reports on the mechanism of chaos. Recently, analyses on energy cycling in chaotic systems have made some progresses. For instance, Vinicio Pelino, Filippo Maimone, and Pasini described the energy cycle of Lorenz attractor [12]. The energy cycle of the Qi four-wing chaotic system [5] was explained by using the system entropy and the Casimir function as the kernel of Lie–Poisson bracket. In this process, the concerned system was converted to Kolmogorov form containing the conservative term, dissipative term, and an external force [5, 12]. As a measuring index of the orbital mode, the rate of change of Casimir energy, Casimir power, is analyzed in detail. The conservative term is interpreted by Euler equations. As a basic equation in inviscid hydrodynamics, Euler equation gives a Hamiltonian description in 3D form. However, higher-dimensional Euler equations (such as 4D and 5D) are essential to be studied.

In research of chaotic systems, an important and useful implementation is encryption algorithms [13–16] because of the complex properties, such as extremely sensitive dependency on initial conditions, topologically mixing and density of periodic orbits, broadband, pseudo-randomness, and white-noise-like phenomenon [16]. Since the first four-dimensional hyperchaotic system [17] was proposed, researchers found that a hyperchaotic system has potential in engineering applications, especially in control [18, 19], encryption [20, 21], communication [22], synchronization [23], optical system [24], and biological network [25]. Research on hyperchaotic systems has become a hot topic. One of the most important phenomena in these dynamical systems [26–28] is the multistability occurring in physics, chemistry, biology [29], economics [30], and nature. There are two kinds of systems with multistability including hidden attractors [31] and infinite attractors [32, 33]. Both display complex dynamical behavior such as the coexistence attractor [11, 34]. All CCSs do not have attractors, but some have line equilibrium which is referred as hidden attractors. Therefore, it is interesting to test whether CCSs can show multistability behavior as well. For application, chaos can be controlled and synchronized, usually including designing a controller to stabilize the chaotic system and tracking the chaotic system. Chaos synchronization is of vital significance to the practical application of chaos. Important works in chaos synchronization for the chaotic system and its applications in control and tracking have been done recently and in the past [35, 36]. Design and implementation of the pseudo-random digital signal generator is one of the most important chaos-based application. With the advantages of digital integrated circuits, superior computing power, and reconfigurable designs [37], FPGA is considered as one of the most suitable platforms to implement a chaotic system.

While intensive research studies were made on 3D and 4D chaotic systems, this paper focuses on the vital importance to expand the research to higher-dimensional systems, for instance, 5D systems, which display rich dynamics and lay an important foundation for higher-dimensional chaotic systems' study.

The rest of this paper is listed as follows: in Section 2, five 5D Euler equations are constructed, and a family of HCCSs are proposed; in Section 3, the nonconservation property of the proposed HCCS and dynamics are analyzed in detail by numerical simulation; in Section 4, adaptive synchronization is achieved for system Σ_3^H; in Section 5, FPGA digital development platform is used to generate the pseudo-random number generator; and Section 6 concludes the paper.

2. Modeling of HCCS

2.1. Model of 5D Euler Equations. Euler equations govern the rotation of a rigid body and control the motion of an inviscid fluid, which are also applicable to incompressible fluid. 5D Euler equations are imperative to satisfy the Lie–Poisson structure. Thus, from the view point of the 3D free rotational rigid body, 5D Euler equations governing the 5D rigid body or fluid systems can be constructed satisfying the Lie–Poisson bracket for the generalized Hamiltonian systems or Kolmogorov systems. In [10], six types Euler equations are proposed but the modeling work just considering the four-dimensional case. On the contrary, only the system dimension of a conservative chaotic system is greater than or equal to 5, and the dynamics of the system may be hyperchaotic state according to the requirements of LEs.

To construct the 5D Euler equations, the following 3D rigid subbodies are considered: subbody S_{ijk} defined in the space spanned from the axes ijk (taking the values of 123, 124, 125, 145, 245, and 345). Suppose there is a 5D rigid body with five axes, with the principle moment of inertia I_i, $\Pi_i = I_i^{-1}$, and angular momentum $x_i = I_i\omega_i$, ω_i is the angular velocity, $i = 1, 2, 3, 4, 5$. Then, the six 3D rigid subbodies can be extended to 5D by leaving another two dimensions uncoupled, and one gets the generalized 5D sub-Euler equations; these six 5D sub-Euler equations can be used to construct the five types of 5D Euler equations as summarized in Table 1.

As an example of Table 1, by coupling subbody S_{123} and subbody S_{345} with the third common axis, the 5D Euler equation of body $\sum_3$ is demonstrated in a Hamiltonian vector field form as equation (1). Bodies $\sum_1$, $\sum_2$, $\sum_4$, and $\sum_5$ can be developed in the similar way. The general form of the five 5D Euler equations is $\sum_i \dot{x} = J_i(x)\nabla H(x)$, where $i = 1, 2, 3, 4,$ and 5.

$$\sum\nolimits_3 \dot{x} = J_3(x)\nabla H(x), \tag{1}$$

with

$$J_3(\mathrm{x}) = \begin{bmatrix} 0 & -x_3 & x_2 & 0 & 0 \\ x_3 & 0 & -x_1 & 0 & 0 \\ -x_2 & x_1 & 0 & 0 & 0 \\ 0 & 0 & 0 & 0 & 0 \\ 0 & 0 & 0 & 0 & 0 \end{bmatrix} + \begin{bmatrix} 0 & 0 & 0 & 0 & 0 \\ 0 & 0 & 0 & 0 & 0 \\ 0 & 0 & 0 & -x_5 & x_4 \\ 0 & 0 & x_5 & 0 & -x_3 \\ 0 & 0 & -x_4 & x_3 & 0 \end{bmatrix} = \begin{bmatrix} 0 & -x_3 & x_2 & 0 & 0 \\ x_3 & 0 & -x_1 & 0 & 0 \\ -x_2 & x_1 & 0 & -x_5 & x_4 \\ 0 & 0 & x_5 & 0 & -x_3 \\ 0 & 0 & -x_4 & x_3 & 0 \end{bmatrix}, \tag{2}$$

and its cross-product form is

Table 1: Modeling coupling mode.

Type	Subbody A	Subbody B	Common axis	Coupled rigid body
1	Subbody S_{123}	Subbody S_{145}	First axis	Body $\sum_1$
2	Subbody S_{123}	Subbody S_{245}	Second axis	Body $\sum_2$
3	Subbody S_{123}	Subbody S_{345}	Third axis	Body $\sum_3$
4	Subbody S_{124}	Subbody S_{345}	Fourth axis	Body $\sum_4$
5	Subbody S_{125}	Subbody S_{345}	Fifth axis	Body $\sum_5$

$$\sum\nolimits_3 \dot{x} = x_{123} \times \nabla H\left(x_{123}\right) + x_{345} \times \nabla H\left(x_{345}\right). \tag{3}$$

The Hamiltonian energy of these 5D systems is

$$H(x) = \frac{1}{2}\left(\Pi_1 x_1^2 + \Pi_2 x_2^2 + \Pi_3 x_3^2 + \Pi_4 x_4^2 + \Pi_5 x_5^2\right). \tag{4}$$

As a significant physical quantity, similiar to the enstrophy or potential vorticity in the context of hydrodynamics, the Casimir function, C, is a valid way in globally describing a dynamical system and analyzing stability conditions. The Casimir function is defined as the kernel of the Lie–Poisson bracket [38]:

$$\{F, H\} = [\nabla F(x)]^T J(x) \nabla H(x), \tag{5}$$

in which $J(x)$ is the structural matrix of a generalized Hamiltonian system, which meets $J(x) = -J^T(x)$, i.e., $\{C, G\} = 0$, $\forall G \in C^{\infty}(g^*)$.

For a Hamiltonian system with a constant of the motion, one gets $\{C, H\} = 0$. The Casimir energy is conservative when there is no dissipative torque and external torque [5, 39]. The Casimir function (energy) of a generalized 5D Euler equations can be defined as

$$C(x) = \frac{1}{2}\left(x_1^2 + x_2^2 + x_3^2 + x_4^2 + x_5^2\right). \tag{6}$$

The rate of change of the Casimir energy is called the Casimir power [10], which is defined as

$$\dot{C} = x^T \cdot \dot{x} = x^T \cdot J(x) \nabla H(x), \tag{7}$$

in which $J(x)$ is an antisymmetric matrix, which represents the energy conservative part of a system.

Remark 1. The constructed 5D Euler equations (Tex translation failed) ($i = 1, 2, 3, 4, 5$) are both Hamiltonian and Casimir energy conservative.

The proposed five 5D Euler equations satisfy the vector field shown in equation (1), which provides the symplectic structure. Because the proposed 5D Euler equations are conservative for both the Hamiltonian and Casimir energy, they cannot produce chaos. However, they can be used as the basic framework to construct the HCCS.

2.2. The Proposed 5D HCCS. To generate chaotic behavior, conservation of the proposed generalized 5D Euler equations has to be broken. Replace one zero element by a in the upper triangle and $-a$ in the lower triangle of $J_i(x)$, respectively. Because $J_i^H(x)$ still keeps the skew-symmetric form, the conservations of Hamiltonian are preserved, but Casimir energy is broken. Correspondingly, the five systems $\sum_i$ generate a family of Hamiltonian conservative chaotic systems:

$$\sum\nolimits_i^H \dot{x} = J_i^H(x) \nabla H(x). \tag{8}$$

As an example, for $J_3^H(x)$, one gets

$$J_3^H(x) = \begin{bmatrix} 0 & -x_3 & x_2 & 0 & 0 \\ x_3 & 0 & -x_1 & a & 0 \\ -x_2 & x_1 & 0 & -x_5 & x_4 \\ 0 & -a & x_5 & 0 & -x_3 \\ 0 & 0 & -x_4 & x_3 & 0 \end{bmatrix}, \tag{9}$$

with a is a constant. The resulting system is a HCCS.

Force and energy analysis can be used to explain the mechanism underlying chaos and its dynamic states [5]. For system Σ_3^H, the Casimir energy is not conservative, which means there must exist an external torque that breaks the conservation. According to Kolmogorov–Arnold–Moser perturbation theorem [10], when a Hamiltonian system whose $H(x)$ function is perturbed by the inclusion of an interaction term $H_1(x)$, the coupled Hamiltonian system probably generates conservative chaos with Hamilton function $H_2(x) = H(x) + \varepsilon H_1(x)$ because of the energy exchange between the two Hamiltonian functions ($H(x)$ and $H_1(x)$).

From equations (8) and (9), we have

$$\sum\nolimits_3^H \dot{x} = J_3(x) \nabla H(x) + J^H(x) \nabla H_1(x), \tag{10}$$

with

$$J^H(x) = \begin{bmatrix} 0 & 0 & 0 & 0 & 0 \\ 0 & 0 & 0 & a & 0 \\ 0 & 0 & 0 & 0 & 0 \\ 0 & -a & 0 & 0 & 0 \\ 0 & 0 & 0 & 0 & 0 \end{bmatrix}, \tag{11}$$

$$H_1(x) = \frac{1}{2}\left(\Pi_2 x_2^2 + \Pi_4 x_4^2\right).$$

Consider $H_1(x)$ as a perturbation term, which represents a kind of external torque. According to equation (7), the Casimir power of system Σ_3^H is

$$\begin{aligned} \dot{C} &= x^T \cdot \dot{x} \\ &= x^T \cdot J_3(x) \nabla H(x) + x^T \cdot J^H(x) \nabla H_1(x) \\ &= a\left(\Pi_4 - \Pi_2\right) x_2 x_4. \end{aligned} \tag{12}$$

The term $J_3(x) \nabla H(x)$ of system Σ_3^H is conservative in both Hamiltonian and Casimir energy. Therefore, this term is an inertial torque, which can be a kind of fictitious torque generated by a free rotational rigid body without external torque [5, 38]. But, the term $J^H(x) \nabla H_1(x) = \begin{bmatrix} 0 & \Pi_4 x_4 & 0 & \Pi_2 x_2 & 0 \end{bmatrix}^T$ is a nonconservative torque and

leads to the loss of Casimir energy conservation. Rewrite system Σ_3^H in vector form to illustrate the conservative and nonconservative torque as

$$\begin{bmatrix} \dot{x}_1 \\ \dot{x}_2 \\ \dot{x}_3 \\ \dot{x}_4 \\ \dot{x}_5 \end{bmatrix} = \begin{bmatrix} (\Pi_3 - \Pi_2)x_2x_3 \\ (\Pi_1 - \Pi_3)x_1x_3 \\ (\Pi_2 - \Pi_1)x_1x_2 + (\Pi_5 - \Pi_4)x_4x_5 \\ (\Pi_3 - \Pi_5)x_3x_5 \\ (\Pi_4 - \Pi_3)x_3x_4 \end{bmatrix} + \begin{bmatrix} 0 \\ a\Pi_4x_4 \\ 0 \\ -a\Pi_2x_2 \\ 0 \end{bmatrix}, \tag{13}$$

where the first vector term on the right is the initial torque, and the second vector term is the external term causing the energy exchanges between dissipative and supplied energy.

3. Dynamic Analysis on the Proposed 5D HCCS

For simplicity, we only analyze system $\sum_3^H$:

$$\sum_3^H: \begin{aligned} \dot{x}_1 &= (\Pi_3 - \Pi_2)x_2x_3 \\ \dot{x}_2 &= (\Pi_1 - \Pi_3)x_1x_3 + a\Pi_4x_4 \\ \dot{x}_3 &= (\Pi_2 - \Pi_1)x_1x_2 + (\Pi_5 - \Pi_4)x_4x_5 \\ \dot{x}_4 &= (\Pi_3 - \Pi_5)x_3x_5 - a\Pi_2x_2 \\ \dot{x}_5 &= (\Pi_4 - \Pi_3)x_3x_4 \end{aligned}. \tag{14}$$

System has six adjustable parameters: Π_i ($i = 1$, 2, 3, 4, and 5) and a having influences on the system dynamic motion. The initial values x_{i0} determine Hamiltonian equation (4) when Π_i is fixed. From equation (12), parameters a and Π_i determine the change rate of Casimir energy, which will impact the degree of chaos with fixed x_{i0}.

3.1. Equilibrium Point Analysis on System Σ_3^H. With $(\Pi_1, \Pi_2, \Pi_3, \Pi_4, \Pi_5, a) = (14, 20, 10, 5, 30, 0.1)$, the equilibrium points of system Σ_3^H are $(p, 0, 0, 0, 0)$, $(0, 0, r, 0, 0)$, $(0, 0, 0, 0, q)$, and $(p, 0, 0, 0, q)$, in which $p, q, r \in R$. Thus, the equilibrium points of system Σ_3^H are in the form of three lines and one plane. Substituting equilibrium points $(0, 0, 0, 0, 0)$, $(p, 0, 0, 0, 0)$, $(0, 0, r, 0, 0)$, $(0, 0, 0, 0, q)$, and $(p, 0, 0, 0, q)$ into the Jacobian matrix and calculating the characteristic polynomial, one gets

$$f_1(\lambda) = \lambda^3 \cdot \left(\lambda^2 + 1\right), \tag{15}$$

$$f_2(\lambda) = \lambda^3 \cdot \left[\lambda^2 + \left(1 - 24 \cdot x_1^2\right)\right], \tag{16}$$

$$f_3(\lambda) = \lambda \cdot \left[\lambda^4 + \left(1 - 60 \cdot x_3^2\right) \cdot \lambda^2 - 4000 \cdot x_3^4\right], \tag{17}$$

$$f_4(\lambda) = \lambda^3 \cdot \left[\lambda^2 + \left(1 + 500 \cdot x_5^2\right)\right], \tag{18}$$

$$f_5(\lambda) = \lambda^2 \cdot \left[\lambda^3 + \left(1 + 500 \cdot x_5^2 - 24 \cdot x_1^2\right) \cdot \lambda + 260 \cdot x_1 \cdot x_5\right], \tag{19}$$

respectively. Let these characteristic polynomials equal to zero; then, we obtain the eigenvalues of these polynomials, as shown in Table 2.

System Σ_3^H has nonhyperbolic equilibrium points, which are rare in chaotic systems [8]. Another finding from Table 2 is that different kinds of equilibrium points all have zero eigenvalues, so the equilibrium points of Σ_3^H are all unstable (exponential) [40].

3.2. Numerical Investigations. Let $(\Pi_1, \Pi_2, \Pi_3, \Pi_4, \Pi_5) = (14, 20, 10, 5, 30)$ and initial values $(x_{10}, x_{20}, x_{30}, x_{40}, x_{50}) = (0.1, 0.5, 0.5, 0.5, 0.1)$. When $a = 0$, system Σ_3^H becomes (Tex translation failed), it is both Hamiltonian energy ($H(t) = 4.595$) and Casimir energy ($C(t) = 0.385$) conservative with a periodic trajectory (the red curve shown in Figure 1), and the Casimir power is zero (the red line in Figure 2). When $a = 0.1$, Σ_3^H is still Hamiltonian conservative ($H(t) = 4.595$) but not Casimir energy, and the Casimir power is not zero as the blue curve shown in Figure 2. The orbit becomes chaotic as shown by the blue trajectory in Figure 1.

Usually, the bifurcation diagram evolution process is "source—periodic orbit—double periodic orbits—multiperiodic orbits—chaos." However, system Σ_3^H does not. It enters the chaotic orbit almost immediately when the parameter $a > 0$, as shown in the bifurcation diagram in Figure 3(a), $a \in [0, 0.01]$; correspondingly, Figure 3(b) shows the Lyapunov exponent spectrum as a increases, in which there are two LEs greater than 0.

Remark 2. When the Casimir energy is conservative, the system may be either periodic or quasi-periodic states.

Considering $\Pi_2 = \Pi_4$ with $a \neq 0$, we have $\dot{C} = a(\Pi_4 - \Pi_2)x_2x_4 = 0$; hence, the system remains conservative both in the Hamiltonian and the Casimir energy with $H(t) = 2.72$ and $C(t) = 0.385$, where $\Pi_2 = \Pi_4 = 5$, $a = 0.1$, and the system is quasi-periodic state with five zero Les; the corresponding phase portrait and Poincare section are shown in Figure 4.

3.3. Coexistence of System Σ_3^H. The dynamics of classical chaotic systems contain periodic motion, quasi-periodic motion, chaos, and hyperchaos, which can be verified by LEs [41, 42]. A hyperchaotic system is characterized by the presence of two or more positive LEs [41, 43]. For a dynamical system with conservative flows, the sum of all LEs must be zero [43]. There must be two positive LEs for a 5D autonomous conservative hyperchaotic system.

Basin of attraction is an important tool for analyzing the dissipative coexisting attractors [44, 45], which change with initial values. Various initial values can be used to get full information about the typical regimes and their localization; as the same idea of the basin of attraction, the dynamical evolution map is used for this purpose.

The dynamical evolution map is generated for system Σ_3^H to study the coexistence phenomenon. Fixed system parameters $(\Pi_1, \Pi_2, \Pi_3, \Pi_4, \Pi_5, a) = (14, 20, 10, 5, 30, 1.5)$, the sampling period = 0.1 s, and changed the third and fourth initial values, i.e., $(0.1, 0.5, x_{30}, x_{40}, 0.1)$, where $x_{30} \in [-8, 8]$ and $x_{40} \in [-5, 5]$, the step of the initial values changing is 0.05. The dynamical evolution map is shown in Figure 5, which shows LE_1, LE_2, LE_4, and LE_5 of each point with

Table 2: Σ_3^H Hamiltonian conservative chaotic system.

System	Equilibrium ($p, q, r \in \mathbb{R}$)	$f(\lambda)$	Eigenvalue ($\sigma, \omega > 0$)	Hyperbolic or not
Σ_3^H	(0, 0, 0, 0, 0)	$f_1(\lambda)$	$(0, 0, 0, j, -j)$	Nonhyperbolic
			$(0, 0, 0, j\omega_1, -j\omega_1)$	Nonhyperbolic
	(p, 0, 0, 0, 0)	$f_2(\lambda)$	$(0, 0, 0, \sigma_1, -\sigma_1)$	Hyperbolic
	(0, 0, r, 0, 0)	$f_3(\lambda)$	$(0, \sigma_2, -\sigma_2, j\omega_2, -j\omega_2)$	Nonhyperbolic
			$(0, 0, 0, j\omega_3, -j\omega_3)$	Nonhyperbolic
	(0, 0, 0, 0, q)	$f_4(\lambda)$	$(0, 0, \sigma_3, -\sigma_4 + j\omega_1, -\sigma_4 - j\omega_1)$	Hyperbolic
			$(0, 0, \sigma_3, \sigma_4 + j\omega_1, \sigma_4 - j\omega_1)$	Hyperbolic
			$(0, 0, 0, j\omega_4, -j\omega_4)$	Nonhyperbolic
			$(0, 0, +\sigma_5, -\sigma_6, -\sigma_7)$	Hyperbolic
	(p, 0, 0, 0, q)	$f_5(\lambda)$	$(0, 0, -\sigma_5, +\sigma_6, +\sigma_7)$	Nonhyperbolic
			$(0, 0, 0, \sigma_8, -\sigma_8)$	Nonhyperbolic

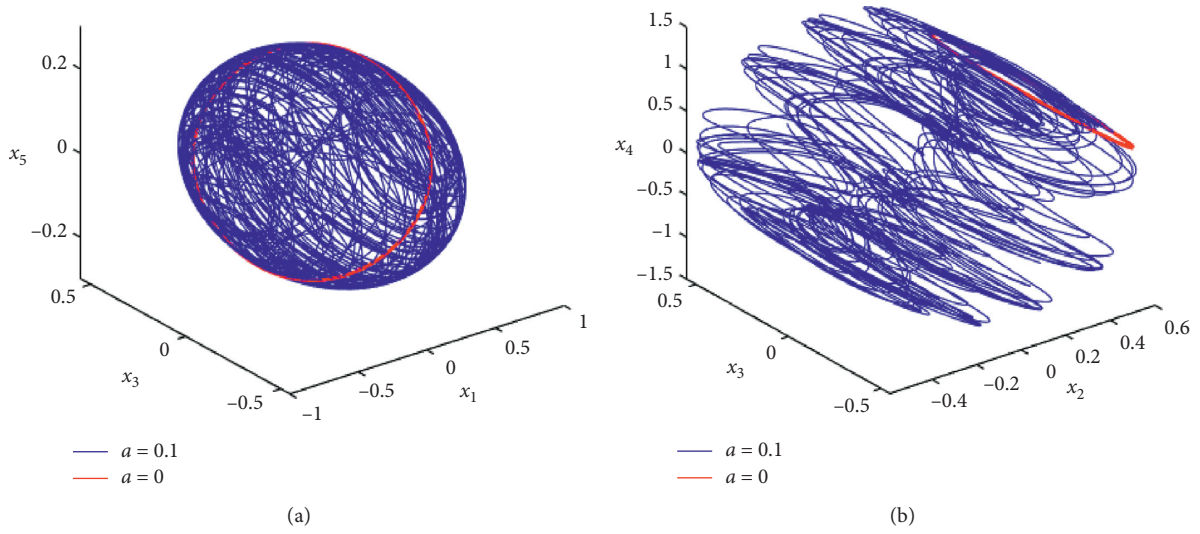

Figure 1: Phase portraits of (a) $x_1 - x_3 - x_5$ and (b) $x_2 - x_3 - x_4$ with $a = 0$ (red orbit) and $a = 0.1$ (blue orbit).

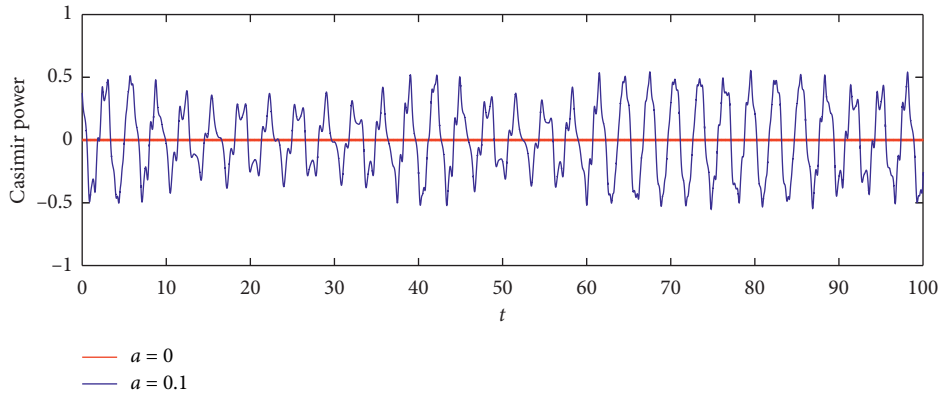

Figure 2: Time series of Casimir power with $(\Pi_1, \Pi_2, \Pi_3, \Pi_4, \Pi_5) = (14, 20, 10, 5, 30)$.

$LE_3 = 0$, respectively. Various coexisting orbits are highlighted with different colors in Figure 4. The values of region A are close to zero. The rest area is denoted as region B, where the values of LEs are greater than zero.

Comparing the dynamical evolution map, one finds that the LEs are symmetric about their 0 LE, and the dynamics of system switch among hyperchaos, chaos, and quasi-periodic motion. When the initial values of x_{30} and x_{40} are located in region A, all of the five LEs are approximating to zero, which indicates the system undergoes a quasi-periodic motion. When the initial values of x_{30} and x_{40} are located in region B, the largest LE is greater larger than zero, and the second one is greater than or equal to zero, which means the system is chaotic or hyperchaotic. As a demonstration, Figures 6 and 7

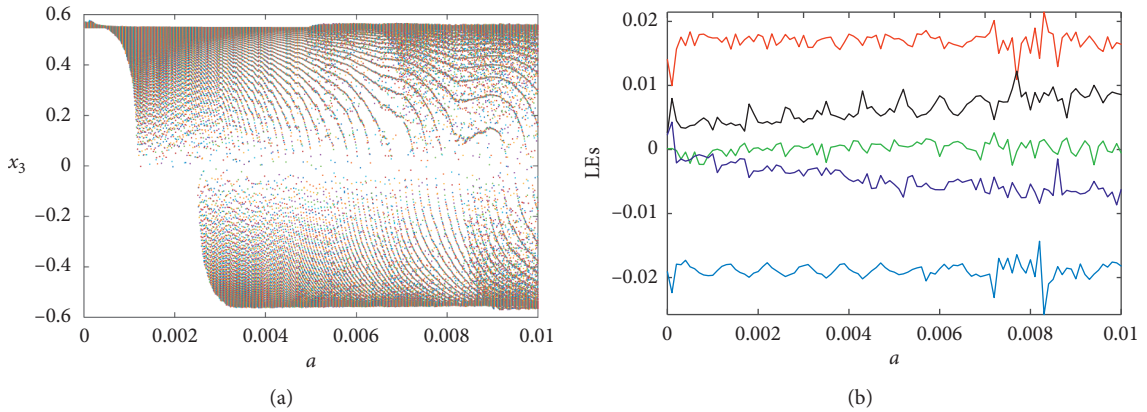

Figure 3: (a) Bifurcation diagram of x_3; (b) Lyapunov exponent spectrum with increase in a.

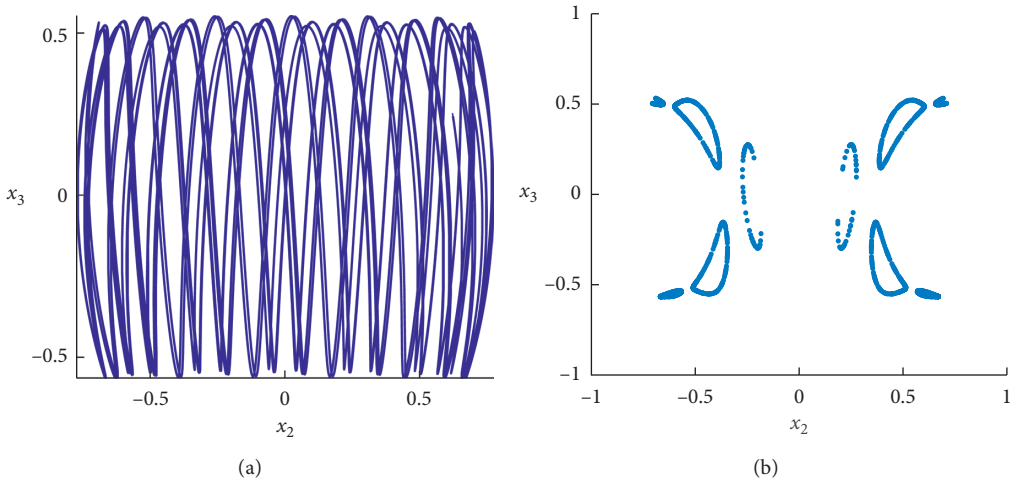

Figure 4: (a) Phase portrait with $\Pi_2 = \Pi_4 = 5, a = 0.1$; (b) Poincare section with $\Pi_2 = \Pi_4 = 5, a = 0.1$.

show the coexistence of quasi-periodic state with $x_{30} = 0.9$, $x_{40} = -3.6$, and hyperchaotic state (with the five LEs 4.4358, 0.1288, 0, −0.1288, and −4.4358) for $x_{30} = 5.5$ and $x_{40} = 0.3$.

When system Σ_3^H evolves into the hyperchaotic state, the system is still Hamiltonian conservative but not in Casimir energy. The phase portraits with Hamiltonian and Casimir energy represented by color are shown in Figures 8(a) and 8(b) which confirm this point. Therefore, the break of the conservation of Casimir energy is an effective indicator of the chaos-generating mechanism.

4. Adaptive Synchronization of System Σ_3^H

The property of chaotic synchronization gives the ability to exercise control over the dynamics of the chaotic system. As a result, such systems are of vital importance for secure communication. In this part, the adaptive synchronization method is used to realize the synchronization. The adaptive synchronization method has a mature theoretical and application basis, which is widely used in the electronic field [36, 46, 47]. This method has the following advantages: small synchronization error, the control intensity can be adjusted adaptively according to the error, and if it is applied to chaotic communication, the security is strong.

Relabeling system Σ_3^H as the master system, one gets

$$\begin{cases} \dot{x}_1 = c_1 x_2 x_3, \\ \dot{x}_2 = c_2 x_1 x_3 + a x_4, \\ \dot{x}_3 = c_3 x_1 x_2 + c_4 x_4 x_5, \\ \dot{x}_4 = c_5 x_3 x_5 - b x_2, \\ \dot{x}_5 = c_6 x_3 x_4, \end{cases} \tag{20}$$

where x_1, x_2, x_3, x_4, x_5 are state variables and $c_1, c_2, c_3, c_4, c_5, c_6, a, b$ are parameters. Consider the slave system as

$$\begin{cases} \dot{y}_1 = c_1 y_2 y_3 + u_1, \\ \dot{y}_2 = c_2 y_1 y_3 + a y_4 + u_2, \\ \dot{y}_3 = c_3 y_1 y_2 + c_4 y_4 y_5 + u_3, \\ \dot{y}_4 = c_5 y_3 y_5 - b y_2 + u_4, \\ \dot{y}_5 = c_6 y_3 y_4 + u_5, \end{cases} \tag{21}$$

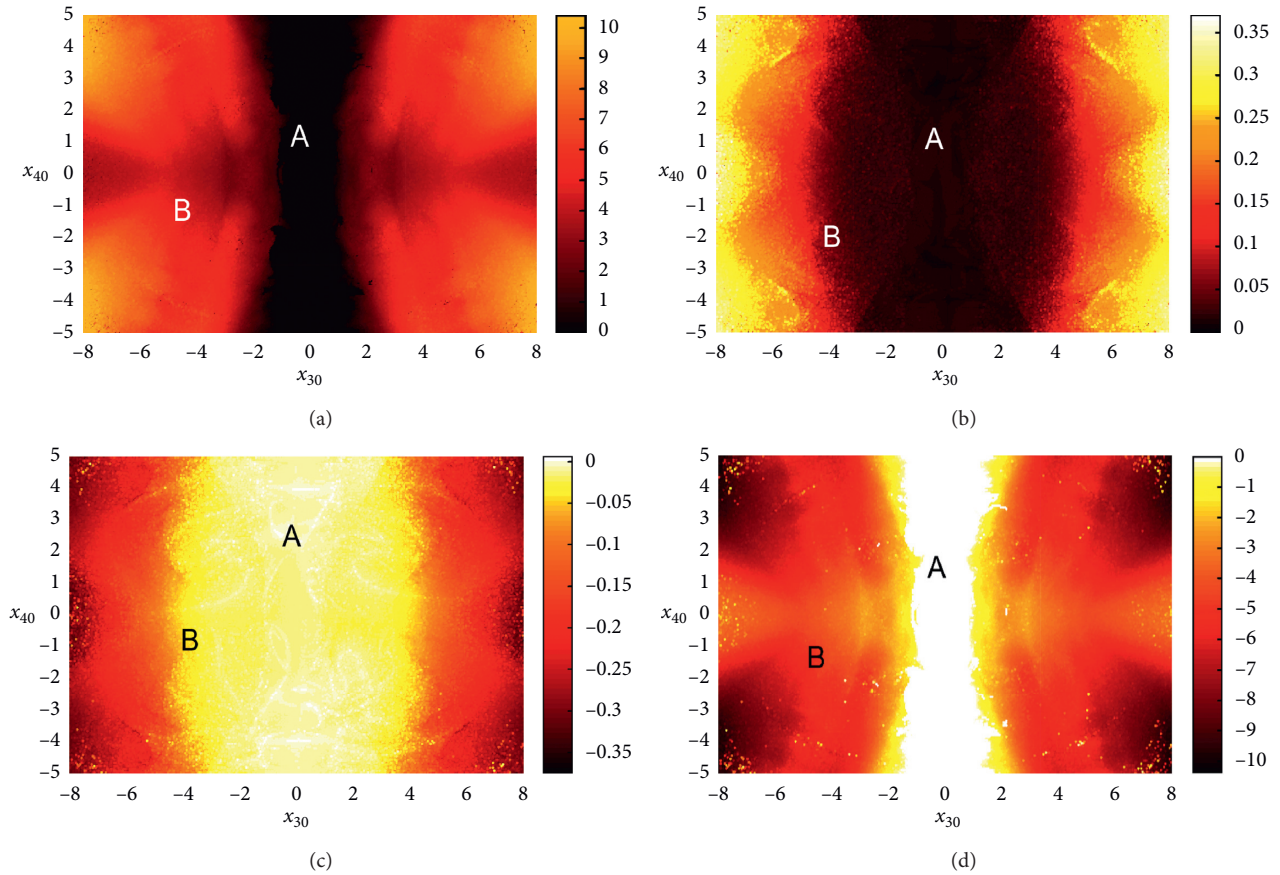

FIGURE 5: Dynamical evolution map in the (x_{30}, x_{40}) plane. (a) LE_1. (b) LE_2. (c) LE_4. (d) LE_5.

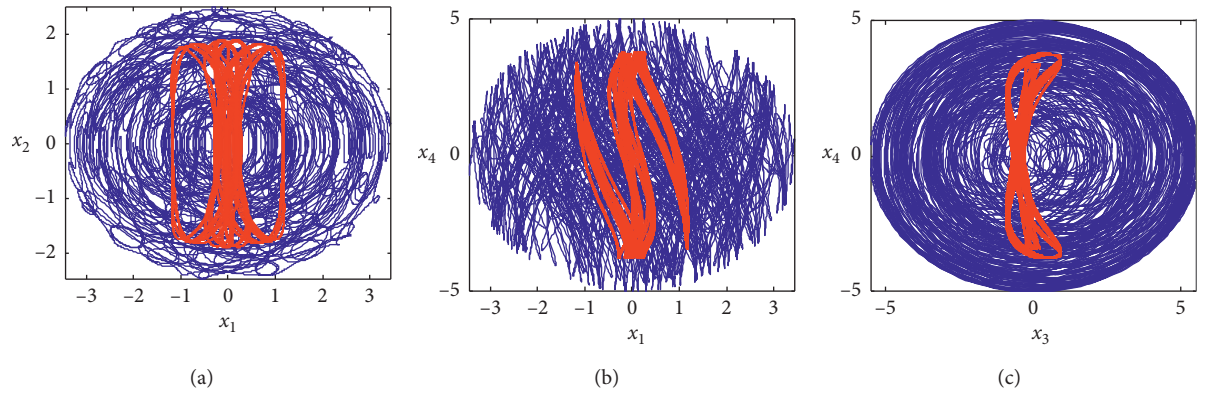

FIGURE 6: Coexistence of the quasi-periodic orbit with $x_{30} = 0.9$ and $x_{40} = -3.6$ (red) and the hyperchaotic orbit with $x_{30} = 5.5$ and $x_{40} = 0.3$ (blue). (a) (x_1, x_2) plane. (b) (x_1, x_4) plane. (c) (x_3, x_4) plane.

where y_1, y_2, y_3, y_4, y_5 are state variables and u_1, u_2, u_3, u_4, u_5 are controllers to be configured. The synchronization errors are determined by $e_i(t) = y_i(t) - x_i(t)$, $i = 1, 2, \ldots, 5$, and the adaptive controllers are set as $u_i = -k_i(y_i - x_i)$, $i = 1, 2, \ldots, 5$, in which $\dot{k}_i = -(y_i - x_i)^2$.

Lyapunov function is constructed as the following form:

$$V = \frac{1}{2}\sum_{i=1}^{5}\left(e_i^2 + k_i^2\right), \quad i = 1, 2, \ldots, 5, \tag{22}$$

and one gets

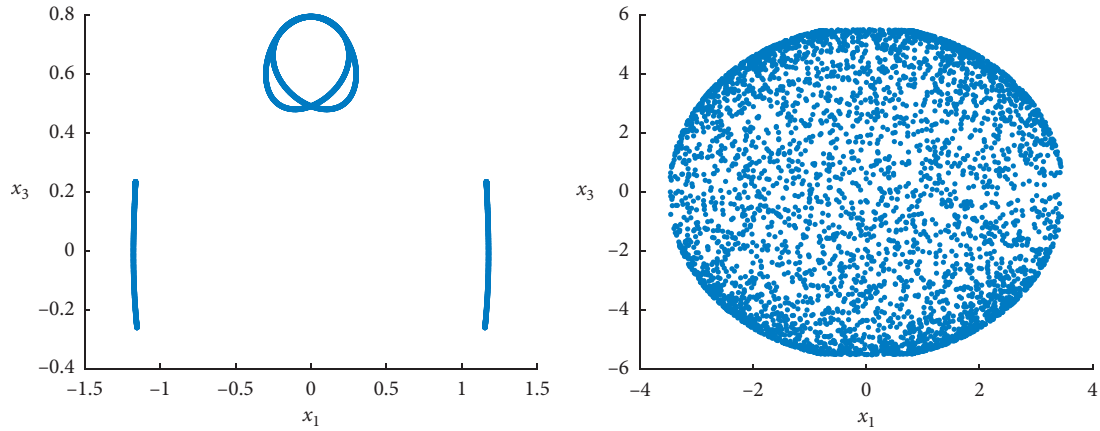

Figure 7: (a) Poincare section of the quasi-periodic orbit with $x_{30} = 0.9$ and $x_{40} = -3.6$; (b) Poincare section of the conservative hyperchaotic orbit with $x_{30} = 5.5$ and $x_{40} = 0.3$.

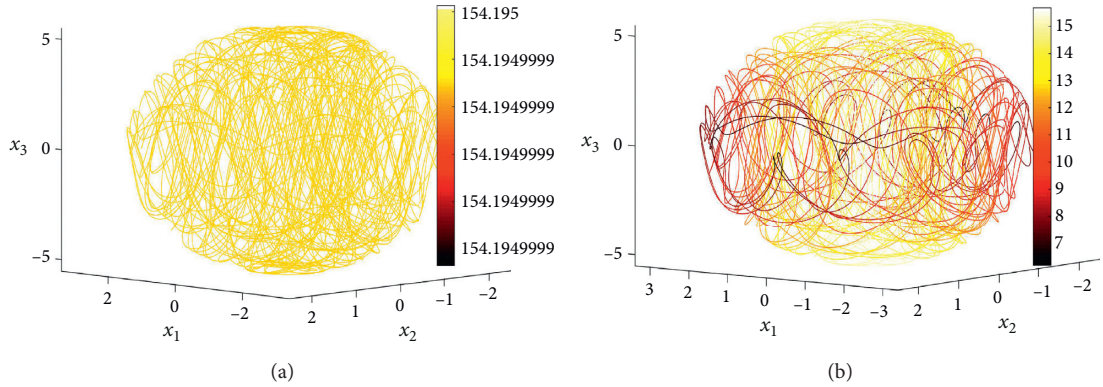

Figure 8: (a) Phase portrait with constant Hamiltonian; (b) phase portrait with varying Casimir energy.

$$\begin{aligned}\dot{V} &= (c_1+c_2)x_3e_1e_2+(c_2+c_3)x_1e_2e_3+(c_1+c_3)x_2e_1e_3\\ &\quad+(c_4+c_5)x_5e_3e_4\\ &\quad+(c_5+c_6)x_3e_4e_5+(c_4+c_6)x_4e_3e_5+(a-b)e_2e_4-2\sum_{i=1}^{5}\left(k_ie_i^2\right)\\ &\le (c_1+c_2)M_{x_3}e_1e_2+(c_2+c_3)M_{x_1}e_2e_3+(c_1+c_3)M_{x_2}e_1e_3\\ &\quad+(c_4+c_5)M_{x_5}e_3e_4\\ &\quad+(c_5+c_6)M_{x_3}e_4e_5+(c_4+c_6)M_{x_4}e_3e_5+(a-b)e_2e_4-2\sum_{i=1}^{5}\left(k_ie_i^2\right)\\ &= -e^TPe,\end{aligned} \tag{23}$$

in which M_{x_i}, $i = 1, 2, \ldots, 5$, are the upper bound of the corresponding state variables, $e = [e_1, e_2, e_3, e_4, e_5]^T$, and P is the matrix corresponding to quadric form $\dot{V}$. Hence, to guarantee the asymptotic stability of synchronization errors, P must be a positive definite matrix, that is to say, $\dot{V}$ is a negative definite quadratic form, which means $e_i \longrightarrow 0$, $i = 1, 2 \ldots 5$ exponentially as times goes on.

Set the control parameters for master system (22) and slave system (23) as $c_1 = -10, c_2 = 4, c_3 = -6, c_4 = 25, c_5 = -20, c_6 = -5$, $a = 7.5$, $b = 30$, the gains $k_1 = 40, k_2 = 40, k_3 = 40, k_4 = 45, k_5 = 50$, and the initial values are $(x_{10}, x_{20}, x_{30}, x_{40}, x_{50}) = (0.1, 0.5, 5.5, 0.3, 0.1)$, under which the master system keeps hyperchaotic states, $(y_{10}, y_{20}, y_{30}, y_{40}, y_{50}) = (1, 0.5, 5, 3, 1)$, respectively. By calculation, matrix P has five positive characteristic roots, and $\dot{V}$ is a negative definite quadratic form. To test the validity of synchronization, simulations are implemented, and the first 5 seconds are time sequences of master and slave systems without synchronization. From the 5th second, synchronization is achieved, see Figures 9(a)–9(c); for the first 5 seconds, x_i and y_i conduct different time evolution, and after synchronization is achieved, x_i and y_i carry on synchronous evolution, and other two variables proceed the similar evolution. Figure 9(d) depicts the time history of e_1, e_2, e_3, e_4, e_5, which converge to 0 quickly, and the state variables move to be synchronized.

5. NIST Test and FPGA Implementation

5.1. NIST Test of System Σ_3^H. The National Institute of Standards and Technology (NIST) provides 15 statistical tests for random or pseudo-random generators, namely, the SP800-22 standard. Widely used in the test of pseudo-random sequences, the SP800-22 standard is considered as a

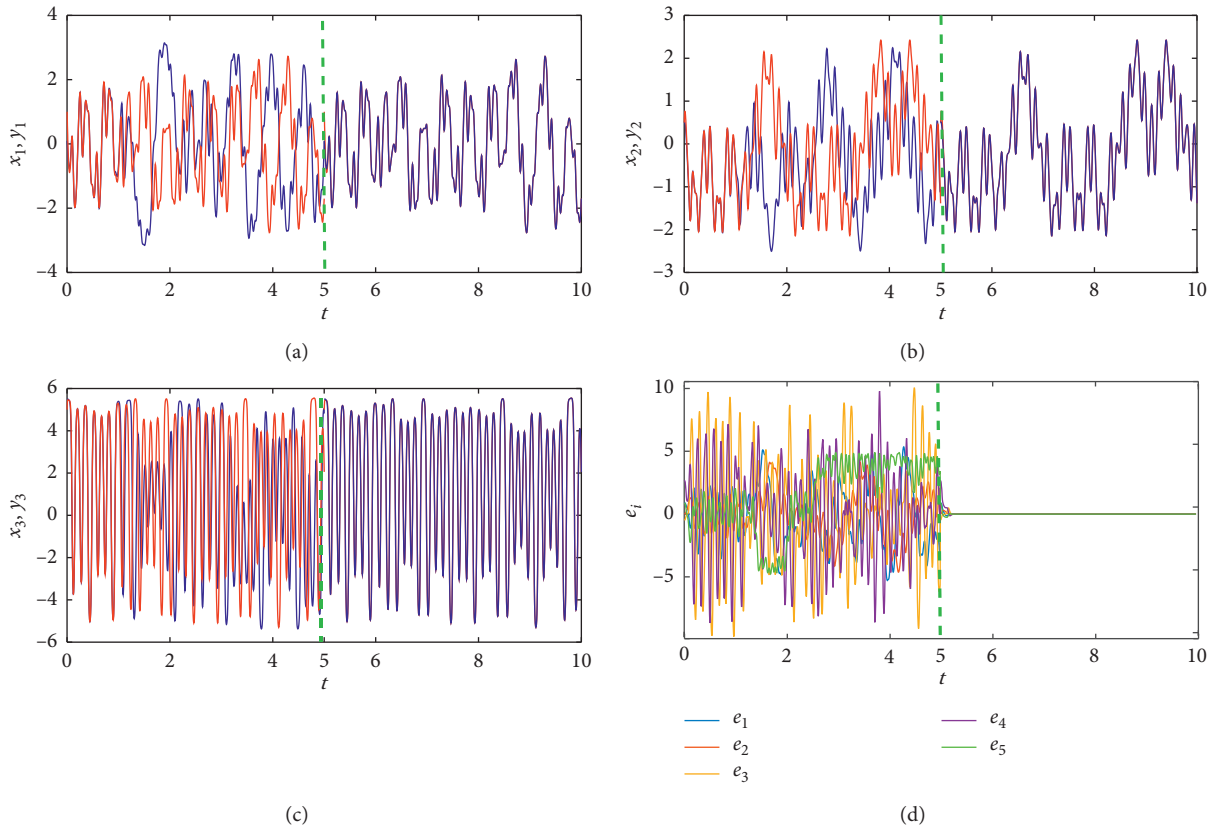

FIGURE 9: Adaptive synchronization simulation results. (a) State variables of x_1(blue); y_1(red). (b) State variables of x_2(blue); y_2(red). (c) State variables of x_3(blue); y_3(red). (d) Time series of synchronization errors.

criterion for evaluating the statistical performance of pseudo-random sequences [48, 49]. The tests comprehensively analyze the performance of the pseudo-random sequence. A sequence passes the test only when the following conditions are satisfied: all P values are greater than the significance level, $\alpha = 0.01$; the relevant proportions are within the acceptance interval $[0.9601, 1.0298]$; and the distribution of P values obeys the uniformity.

From Table 3, all P values obtained in the statistical tests are greater than the significance level, $\alpha = 0.01$, so condition one is met. The relevant proportions lie within the acceptance interval $[0.9601, 1.0298]$, and hence, the second condition holds. In addition, the distribution of P values must pass the uniformity test. For simplicity, we consider the nonoverlapping template (Test No. 8 in Table 3) as an example. The distribution of P values is examined to validate the uniformity which can be visually illustrated using the histogram. Figure 10 shows the distribution of P values for the nonoverlapping template which is uniform. Other 14 tests obtained a similar uniformity. Therefore, the third condition is also satisfied. The conclusion is that the proposed Hamiltonian conservative hyperchaotic system Σ_3^H is suitable as a pseudo-random generator.

5.2. FPGA Implementation for System Σ_3^H. Although some important works have been implemented on FPGA [37, 50], hardware implementation of conservative chaotic systems is more difficult than common dissipative chaotic systems since the former is highly sensitive to initial conditions and computational errors. In this section, we perform the implementation of system Σ_3^H, as an example, based on the FPGA platform. In order to accommodate digital computers, the first-order difference algorithm is used to discrete the system [51]. For system Σ_3^H with $(\Pi_1, \Pi_2, \Pi_3, \Pi_4, \Pi_5, a) = (14, 20, 10, 5, 30, 1.5)$, one obtains

TABLE 3: NIST test results of hyperchaotic system Σ_3^H.

No.	Statistical test	P value	Proportion
1	Frequency	0.334538	0.99
2	Block frequency	0.883171	1
3	Cumulative sums	0.637119	0.99
4	Runs	0.798139	1
5	Longest run	0.719747	0.98
6	Rank	0.153763	1
7	FFT	0.096578	0.98
8	Nonoverlapping template	0.437274	0.99
9	Overlapping template	0.595549	0.97
10	Universal	0.955835	1
11	Approximate entropy	0.181557	1
12	Random excursions	0.834308	1
13	Random excursion variant	0.671779	1
14	Serial	0.494392	0.98
15	Linear complexity	0.851383	0.99

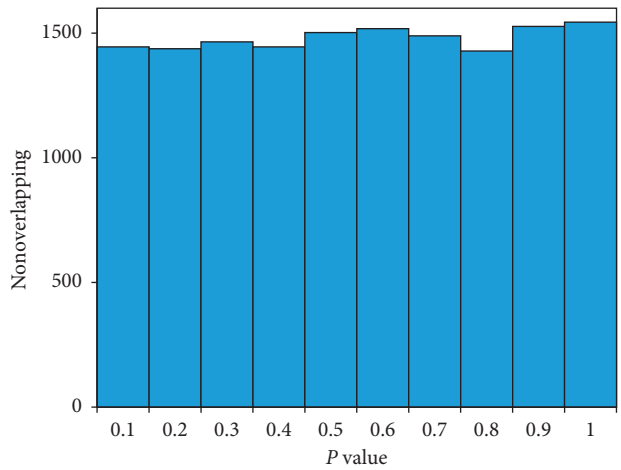

Figure 10: Probability distribution of P value for the nonoverlapping template.

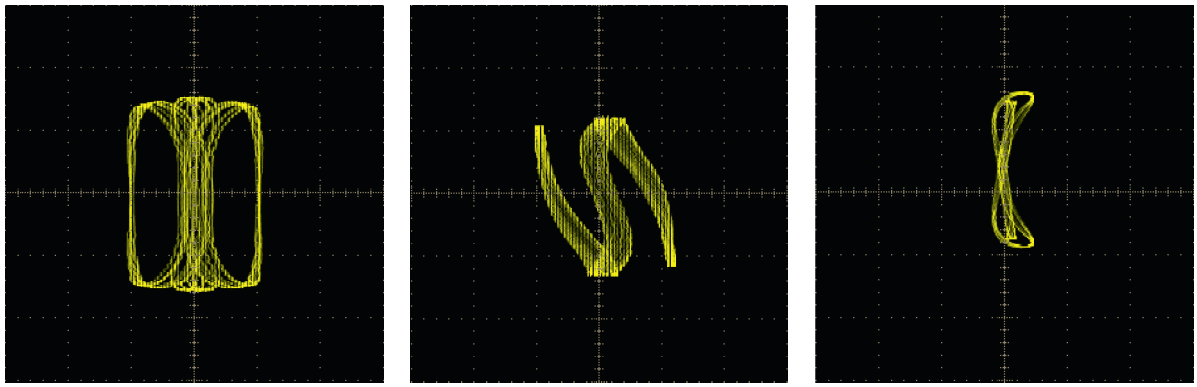

(a) (b) (c)

Figure 11: Quasi-periodic orbit of system Σ_3^H generated by FPGA. (a) (x_1, x_2) plane. (b) (x_1, x_4) plane. (c) (x_3, x_4) plane.

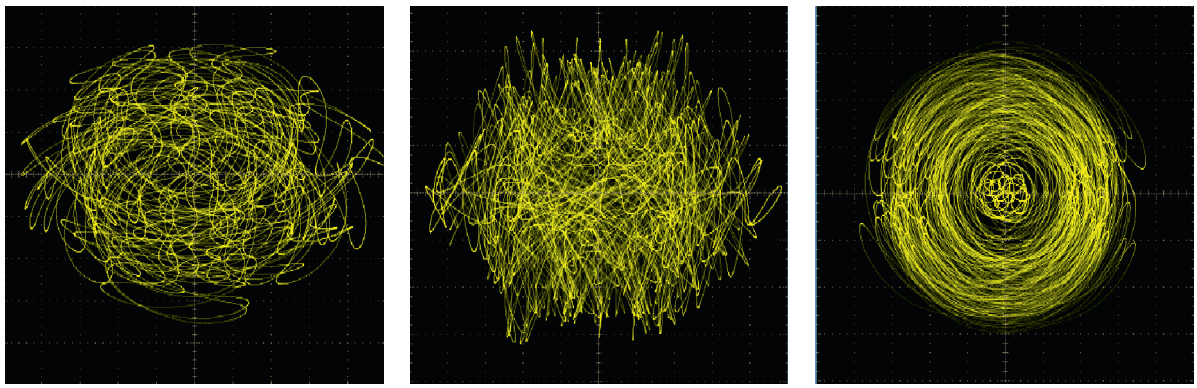

(a) (b) (c)

Figure 12: Hyperchaotic attractor of system Σ_3^H generated by FPGA. (a) (x_1, x_2) plane. (b) (x_1, x_4) plane. (c) (x_3, x_4) plane.

$$\begin{cases} x_1(k+1) = [(\Pi_3 - \Pi_2)x_2(k)x_3(k)]\Delta T + x_1(k), \\ x_2(k+1) = [(\Pi_1 - \Pi_3)x_1(k)x_3(k) + a\Pi_4 x_4(k)]\Delta T + x_2(k), \\ x_3(k+1) = [(\Pi_2 - \Pi_1)x_1(k)x_2(k) + (\Pi_5 - \Pi_4)x_4(k)x_5(k)]\Delta T + x_3(k), \\ x_4(k+1) = [(\Pi_3 - \Pi_5)x_3(k)x_5(k) - a\Pi_2 x_2(k)]\Delta T + x_4(k), \\ x_5(k+1) = [(\Pi_4 - \Pi_3)x_3(k)x_4(k)]\Delta T + x_5(k). \end{cases} \quad (24)$$

The discrete model was built by DSP-builder in MATLAB (R2015b). Then, system (24) is solved by the fourth-order the Runge–Kutta method in Matlab/Simulink/DSP-builder, with the fixed step of 10^{-8} s, initial values set as Section 3.3, and sampling time of 10^{-6} s. The system models in equation (24) are converted to the VHDL code (Verilog hardware description language), synthesized, and compiled to the RTL (register transfer level) code.

To compare the results of computer simulation with digital circuit implementation, the phase portraits of system Σ_3^H are shown in Figures 11 and 12. It shows that the phase portraits of system Σ_3^H implemented by FPGA are roughly consistent with the computer simulation (shown in Figure 5), which means the conservative hyperchaotic system is implemented in the digital circuit with an acceptable error level.

6. Conclusions

This paper constructed a family of 5D Hamiltonian conservative hyperchaotic systems. Some interesting properties are revealed by theoretical and numerical analyses. The paper started from extending the 3D Euler equations of rigid bodies to generalized 5D sub-Euler equations. Five 5D Euler equations were then obtained by combining any two of the generalized 5D sub-Euler equations that with one common axis. These 5D Euler equations were proved to be both Hamiltonian and Casimir energy conservative, which can be regarded as the conservative term in a Kolmogorov system or a 5D generalized Hamiltonian system because of their antisymmetric structure matrix. So, these generalized 5D Euler equations are useful to study the dynamics of inviscid fluid and quantum mechanics and rigid body dynamics systems.

The mechanism of the proposed 5D Hamiltonian conservative chaotic systems was found by analyzing the Casimir energy and the Casimir power, which is an effective indicator of chaos generating. Using the dynamical evolution map, the coexistence of quasi-periodic and hyperchaotic was revealed, which showed the abundant dynamic characteristics of the proposed 5D Hamiltonian conservative chaotic systems. By the adaptive synchronization method, the hyperchaotic system was synchronized effectively.

To validate the application value of the proposed systems, NIST tests on system Σ_3^H were performed to verify the feasibility as a random number sequence generator. The system is implemented based on FPGA digital development platform, which was a contributing work for this field due to the difficulties of hardware implementation of conservative hyperchaos. These proposed systems are expected to be further helpfully applied to secure communication, neural network, and economics.

Data Availability

The data used to support the conclusions of this article can be computed by the relative equations and parameters given in the article using ODE45 solver in Matlab.

Conflicts of Interest

The authors declare that there are no conflicts of interest regarding the publication of this paper.

Authors' Contributions

Enzeng Dong and Xiaodong Jiao contributed equally to this work.

Acknowledgments

This work was partially supported by the Natural Science Foundation of China (no. 61873186) and the Natural Science Foundation of Tianjin (no. 18JCYBJC87700).

References

[1] E. N. Lorenz, "Deterministic nonperiodic flow," *Journal of the Atmospheric Sciences*, vol. 20, no. 2, pp. 130–141, 1963.

[2] A. Gragnani and S. Rinaldi, "A universal bifurcation diagram for seasonally perturbed predator-prey models," *Bulletin of Mathematical Biology*, vol. 57, no. 5, pp. 701–712, 1995.

[3] E. Dong, M. Yuan, C. Zhang, J. Tong, Z. Chen, and S. Du, "Topological horseshoe analysis, ultimate boundary estimations of a new 4D hyperchaotic system and its fpga implementation," *International Journal of Bifurcation and Chaos*, vol. 28, no. 7, Article ID 1850081, 2018.

[4] E. Dong, Z. Zhang, M. Yuan, Y. Ji, X. Zhou, and Z. Wang, "Ultimate boundary estimation and topological horseshoe analysis on a parallel 4D hyperchaotic system with any number of attractors and its multi-scroll," *Nonlinear Dynamics*, vol. 95, no. 4, pp. 3219–3236, 2019.

[5] H. Jia, Z. Guo, S. Wang, and Z. Chen, "Mechanics analysis and hardware implementation of a new 3D chaotic system," *International Journal of Bifurcation and Chaos*, vol. 28, no. 13, Article ID 1850161, 2019.

[6] G. Qi and X. Liang, "Mechanism and energy cycling of the Qi four-wing chaotic system," *International Journal of Bifurcation and Chaos*, vol. 27, no. 12, Article ID 1750180, 2017.

[7] W. G. Hoover, "Remark on some simple chaotic flows," *Physical Review E*, vol. 51, no. 1, pp. 759-760, 1995.

[8] A. G. Wu, S. J. Cang, R. Zhang, Z. Wang, and Z. Chen, "Hyperchaos in a conservative system with nonhyperbolic fixed points," *Complexity*, vol. 2018, Article ID 9430637, 8 pages, 2018.

[9] E. Ott, *Chaos in Dynamical Systems*, Cambridge University Press, Cambridge, UK, 2002.

[10] G. Qi, "Modelings and mechanism analysis underlying both the 4D euler equations and Hamiltonian conservative chaotic systems," *Nonlinear Dynamics*, vol. 95, no. 3, pp. 2063–2077, 2018.

[11] E. Dong, M. Yuan, S. Du, and Z. Chen, "A new class of Hamiltonian conservative chaotic systems with multistability and design of pseudo-random number generator," *Applied Mathematical Modelling*, vol. 73, no. 9, pp. 40–71, 2019.

[12] V. Pelino, F. Maimone, and A. Pasini, "Energy cycle for the lorenz attractor," *Chaos, Solitons & Fractals*, vol. 64, no. 1, pp. 67–77, 2014.

[13] F. Sun, S. Liu, Z. Li, and Z. Lü, "A novel image encryption scheme based on spatial chaos map," *Chaos, Solitons & Fractals*, vol. 38, no. 3, pp. 631–640, 2008.

[14] Z. Guan, F. Huang, and W. Guan, "Chaos-based image encryption algorithm," *Physics Letters A*, vol. 346, no. 1–3, pp. 153–157, 2005.

[15] G. Chen, Y. Mao, and C. K. Chui, "A symmetric image encryption scheme based on 3d chaotic cat maps," *Chaos, Solitons & Fractals*, vol. 21, no. 3, pp. 749–761, 2004.

[16] Q. H. Zhang, H. Zhang, and Z.-H. Li, "One-way hash function construction based on conservative chaotic systems," in *Proceedings of the International Conference on Information Assurance Security*, IEEE, Xi'an, China, August 2009.

[17] O. E. Rossler, "An equation for hyperchaos," *Physics Letters A*, vol. 71, no. 2-3, pp. 155–157, 1979.

[18] J. Zheng, "A simple universal adaptive feedback controller for chaos and hyperchaos control," *Computers & Mathematics with Applications*, vol. 61, no. 8, pp. 2000–2004, 2011.

[19] H. Yu, G. Cai, and G. Li, "Dynamic analysis and control of a new hyperchaotic finance system," *Nonlinear Dynamics*, vol. 67, no. 3, pp. 2171–2182, 2012.

[20] G. Qi and S. B. Matondo, "Hyper-chaos encryption using convolutional masking and model free unmasking," *Chinese Physics B*, vol. 23, no. 5, Article ID 050507, 2014.

[21] D. P. Rosin, *Dynamics of Complex Autonomous Boolean Networks*, Springer International Publishing, Berlin, Germany, 2015.

[22] F. Yu, Z. N. Zhang, L. Liu et al., "Secure communication scheme based on a new 5D multistable four-wing memristive hyperchaotic system with disturbance inputs," *Complexity*, vol. 2020, Article ID 5859273, 16 pages, 2020.

[23] S. Vaidyanathan and S. Sampath, "Hybrid synchronization of hyperchaotic chen systems via sliding mode control," in *Lecture Notes of the Institute for Computer Sciences, Social Informatics and Telecommunications Engineering*, vol. 85, pp. 257–266, Springer, Berlin, Germany, 2012.

[24] M. Zhang, T. Liu, P. Li, A. Wang, J. Zhang, and Y. Wang, "Generation of broadband chaotic laser using dual-wavelength optically injected fabry-pérot laser diode with optical feedback," *IEEE Photonics Technology Letters*, vol. 23, no. 24, pp. 1872–1874, 2011.

[25] A. V. Holden and L. F. Olsen, "Exploring nature's roulette wheel: chaos in biological systems," in *Cell to Cell Signals in Plants and Animals*, vol. 51, pp. 173–185, Springer, Berlin, Germany, 1991.

[26] A. Silchenko, T. Kapitaniak, and V. Anishchenko, "Noise-enhanced phase locking in a stochastic bistable system driven by a chaotic signal," *Physical Review E*, vol. 59, no. 2, pp. 1593–1599, 1999.

[27] V. T. Pham, S. Jafari, C. Volos, X. Wang, and S. M. R. H. Golpayegani, "Is that really hidden? The presence of complex fixed-points in chaotic flows with no equilibria," *International Journal of Bifurcation and Chaos*, vol. 24, no. 11, Article ID 1450146, 2015.

[28] P. Jaros, P. Perlikowski, and T. Kapitaniak, "Synchronization and multistability in the ring of modified Rössler oscillators," *The European Physical Journal Special Topics*, vol. 224, no. 8, pp. 1541–1552, 2015.

[29] D. Angeli, J. E. Ferrell, and E. D. Sontag, "Detection of multistability, bifurcations, and hysteresis in a large class of biological positive-feedback systems," *Proceedings of the National Academy of Sciences*, vol. 101, no. 7, pp. 1822–1827, 2004.

[30] M. Peng, Z. Jiang, X. Jiang, J. Hu, and Y. Qu, "Multistability and complex dynamics in a simple discrete economic model," *Chaos, Solitons & Fractals*, vol. 41, no. 2, pp. 671–687, 2009.

[31] V.-T. Pham, S. Jafari, C. Volos, and T. Kapitaniak, "Different families of hidden attractors in a new chaotic system with variable equilibrium," *International Journal of Bifurcation and Chaos*, vol. 27, no. 9, Article ID 1750138, 2017.

[32] J. C. Sprott, S. Jafari, A. J. M. Khalaf, and T. Kapitaniak, "Megastability: coexistence of a countable infinity of nested attractors in a periodically-forced oscillator with spatially-periodic damping," *The European Physical Journal Special Topics*, vol. 226, no. 9, pp. 1979–1985, 2017.

[33] S. Cang, Y. Li, R. Zhang, and Z. Wang, "Hidden and self-excited coexisting attractors in a lorenz-like system with two equilibrium points," *Nonlinear Dynamics*, vol. 95, no. 1, pp. 381–390, 2019.

[34] J. C. Sprott, X. Wang, and G. Chen, "Coexistence of point, periodic and strange attractors," *International Journal of Bifurcation and Chaos*, vol. 23, no. 5, Article ID 1350093, 2013.

[35] L. Ren and G. Zhang, "Adaptive projective synchronization for a class of switched chaotic systems," *Mathematical Methods in the Applied Sciences*, vol. 42, no. 18, pp. 6192–6204, 2019.

[36] T.-L. Liao and S.-H. Tsai, "Adaptive synchronization of chaotic systems and its application to secure communications," *Chaos, Solitons & Fractals*, vol. 11, no. 9, pp. 1387–1396, 2000.

[37] I. Koyuncu, A. T. Ozcerit, and I. Pehlivan, "Implementation of FPGA-based real time novel chaotic oscillator," *Nonlinear Dynamics*, vol. 77, no. 1-2, pp. 49–59, 2014.

[38] J. E. Marsden and T. S. Ratiu, *Introduction to Mechanics and Symmetry: A Basic Exposition of Classical Mechanical Systems*, Springer, Berlin, Germany, 2008.

[39] G. Qi and J. Hu, "Force analysis and energy operation of chaotic system of permanent-magnet synchronous motor," *International Journal of Bifurcation and Chaos*, vol. 27, no. 14, Article ID 1750216, 2017.

[40] Y. A. Kuznetsov, "Elements of applied bifurcation theory," *Applied Mathematical Sciences*, vol. 288, no. 2, pp. 715–730, 2004.

[41] A. Wolf, J. B. Swift, H. L. Swinney, and J. A. Vastano, "Determining lyapunov exponents from a time series," *Physica D: Nonlinear Phenomena*, vol. 16, no. 3, pp. 285–317, 1985.

[42] S. Vaidyanathan and A. T. Azar, *Analysis and Control of a 4-D Novel Hyperchaotic System: Chaos Modeling and Control Systems Design*, Springer International Publishing, Berlin, Germany, 2015.

[43] A. T. Azar, S. Vaidyanathan, and A. Ouannas, *Fractional Order Control and Synchronization of Chaotic Systems: Studies in Computational Intelligence*, Springer, Berlin, Germany, 2017.

[44] C. A. Jousseph, T. S. Kruger, C. Manchein, S. R. Lopes, and M. W. Beims, "Weak dissipative effects on trajectories from the edge of basins of attraction," *Physica A: Statistical Mechanics and Its Applications*, vol. 456, pp. 68–74, 2016.

[45] J. Aguirre, J. C. Vallejo, and M. A. F. Sanjuan, "Wada basins and unpredictability in Hamiltonian and dissipative systems," *International Journal of Modern Physics B*, vol. 17, no. 22, pp. 4171–4175, 2003.

[46] Y. Hong, H. Qin, and G. Chen, "Adaptive synchronization of chaotic systems via state or output feedback control," *International Journal of Bifurcation and Chaos*, vol. 11, no. 4, pp. 1149–1158, 2001.

[47] S. Vaidyanathan, "Qualitative analysis, adaptive control and synchronization of a seven-term novel 3-D chaotic system with a quartic nonlinearity," *International Journal of Control Theory and Applications*, vol. 7, no. 1, pp. 1–20, 2014.

[48] O. Y. Lui, C. H. Yuen, and K. W. Wong, "A pseudo-random number generator employing multiple RNYI maps,"

International Journal of Modern Physics C, vol. 24, no. 11, pp. 44–54, 2013.

[49] A. Rukhin, J. Soto, N. James et al., "A statistical test suite for random and pseudorandom number generators for cryptographic applications," *Applied Physics Letters*, vol. 22, no. 7, pp. 1645–1579, 2001.

[50] G. Y. Wang, X. L. Bao, and Z. L. Wang, "Design and FPGA Implementation of a new hyperchaotic system," *Chinese Physics B*, vol. 17, no. 10, pp. 3596–3602, 2008.

[51] E. Dong, Z. Liang, S. Du, and Z. Chen, "Topological horseshoe analysis on a four-wing chaotic attractor and its FPGA implement," *Nonlinear Dynamics*, vol. 83, no. 1-2, pp. 623–630, 2016.